An Analysis of Cloud Drop Growth by Collection: Part III. Accretion and Self-collection

EDWIN X BERRY[1]

National Science Foundation, Washington, D. C. 20550

RICHARD L. REINHARDT

Sierra Nevada Corporation, Reno, Nev. 89507

(Manuscript received 29 January 1974, in revised form 23 July 1974)

ABSTRACT

Accretion is shown to have a narrowing effect on the drop size distribution while the newly defined processes "large hydrometeor self-collection," is shown to be responsible for the rapid growth of large hydrometeors and observed broadening of drop distribution. Both processes are given parameterizations in terms of rate equations and coefficients.

1. Introduction

In an early parameterization of cloud drop growth which has since been successfully used in several numerical cloud models, Kessler (1969) hypothesized that the more essential features of warm cloud microphysics relevant to the development of precipitation could be represented by two size categories, the smaller "cloud" droplets having insignificant terminal velocities and the larger "hydrometeor" drops having significant terminal velocities; and two growth processes, autoconversion and accretion. Considering the lack of quantitative information about the nature of droplet collection available at the time in the early 1960's that Kessler formed his parameterization, it is a tribute to his insight that the studies reported now lend credibility to the basic accuracy of his parameterization.

The present results supplement the parameterization of Kessler in four basic ways. First, the natural size boundary between the cloud droplets [the small hydrometeor portion of the spectrum ($S1$)] and the larger hydrometeors ($S2$) has been more distinctly specified (Part I, Berry and Reinhardt, 1974a), not on the basis of terminal speeds but rather on the basis of the influence of the collection kernel, as being near 50 μm radius. Second, an additional process, "large-hydrometeor self-collection," has been identified as the process responsible for the broadening and rapid growth of the large hydrometeor spectrum. Third, two theoretical moments of the distribution which result in the common "mean radius" and the newer "predominant radius" are incorporated into the parameterization. In addition, the predominant radius for the large-hydrometeor spectrum is suggested to be more meaningful, both theoretically and experimentally, than the "median volume diameter" which it replaces in the Kessler parameterization. Fourth, parameterized rate equations are here given as functions of the collection kernel, eliminating the need to evaluate arbitrary coefficients.

One important result of having two, rather than one, modes for large-hydrometeor growth is that the spreading need no longer be artificially tied to mean drop growth, as was required in the earlier method and accomplished by constraining the spectrum to fit a Marshall-Palmer distribution. With this constraint removed the present parameterization allows the simulated drops to develop in a more realistic way with account of previously unrepresented feedback features. This dual mode of large-hydrometeor growth also makes possible a more realistic parameterized simulation of the ice phase, which has distinctly different self-collection properties than water, and interacting ice-water phases.

In the present paper a mathematical structure is developed which is compatible with the data of Part II (Berry and Reinhardt, 1974b) and which provides insight into the features of particle growth by collection.

Among the more interesting results of this analysis is the finding that drop "self-collection" can be well represented by the capture of the "predominant" sized drop by one of 1.5 times its diameter.

The following derivations are stepping stones to the formation of a total pattern of parameterization for stochastic collection.

[1] Present affiliation: National Science Foundation, Western Projects Office, Burlingame, Calif. 90410.

2. Mathematical definitions[2]

The drop or particle spectrum is represented by three extensive variables and two intensive variables:

$$N=\int f\langle x\rangle dx \tag{1}$$

$$L=\int xf\langle x\rangle dx \tag{2}$$

$$Z=\int x^2 f\langle x\rangle dx \tag{3}$$

$$x_f=L/N \tag{4}$$

$$x_g=Z/L. \tag{5}$$

The parameter x_f is referred to as the "mean mass" and x_g as the "predominant mass," of the spectrum.

By representing the mass parameters in terms of the mass expectations values in the spectrum, they can specify the spectrum's relative variance:

$$x_f=\langle x\rangle, \tag{6}$$

$$x_g=\langle x^2\rangle/\langle x\rangle, \tag{7}$$

$$\text{var } x=(x_g-x_f)/x_f. \tag{8}$$

Finally, the equations used to specify the rate of change of the spectrum due to stochastic collection are

$$\partial f\langle x\rangle/\partial t=\int_{x_0}^{x/2} f\langle x-x'\rangle V(x-x'|x')f\langle x'\rangle dx' - \int_{x_0}^{\infty} f\langle x\rangle V(x|x')f\langle x'\rangle dx', \tag{9}$$

$$V(r|r')=\pi r^2 V_c^2(r,r')\Delta v(r,r'). \tag{10}$$

These ten equations form the basis for the parameterizations and conclusions that follow.

3. Accretion

Although a familiar term, accretion is not a clearly defined term from the viewpoint of the growth of a total spectrum. Its parameterization is distinctly more complicated than that for self-collection, which will be described in the next section. The difficulty arises from the large variation in collection rates of $S2$ for $S1$ which occur over different parts of $S2$. This leads to changes in the shape of $S2$ and consequent changes in the parameters of $S2$.

In the case of a single drop, or of N_2 drops of identical size, accretion has a clear interpretation: the rate of change of L_2 is just equal to $N_2\,dx_2/dt$. Since x_{f2} and x_{g2} are equal to x_2, the changes of all of the $S2$ parameters have an exact derivation. As we proceed to a broadened spectrum, however, we must take account of the changing shape of $S2$. We shall see that the accretion process does not include the spreading of $S2$ due to the stochastic nature of the collection of droplets from $S1$.

Accretion is defined to occur via the continuous collection mode which is the limit of the stochastic process when $x_2 \gg x_1$. In this limit Eq. (9) may be reduced as follows:

$$\frac{\partial f\langle x_2\rangle}{\partial t}=\int_{S1} f\langle x_2-x_1\rangle V(x_2-x_1|x_1)f\langle x_1\rangle dx_1 - \int_{S1} f\langle x_2\rangle V(x_2|x_1)f\langle x_1\rangle dx,$$

$$=\int_{S1}\left[f\langle x_2-x_1\rangle V(x_2-x_1|x_1) - f\langle x_2\rangle V(x_2|x_1)\right]f\langle x_1\rangle dx,$$

$$=-\int_{S1} x_1\frac{\partial}{\partial x_2}\left[f\langle x_2\rangle V(x_2|x_1)\right]f\langle x_1\rangle dx,$$

$$=-\frac{\partial}{\partial x_2}\left[f\langle x_2\rangle\int_{S1} V(x_2|x_1)f\langle x_1\rangle dx_1\right], \tag{11}$$

$$=-\frac{\partial}{\partial x_2}\left[f\langle x_2\rangle\frac{dx_2}{dt}\right], \tag{12}$$

where the integral in (11) is the continuous growth rate of drops in $S2$. Thus,

$$\frac{dx_2}{dt}=\int_{S1} V(x_2|x_1)x_1 f\langle x_1\rangle dx_1. \tag{13}$$

When $S1$ is sufficiently narrow this becomes

$$\frac{dx_2}{dt}=V(x_2|x_1)L_1. \tag{14}$$

There is no ambiguity in the interpretation of (13) and (14) since these equations deal with the distinct drop sizes x_2.

The corresponding changes in N_2, L_2 and Z_2 for a broadened $S2$ spectrum may be derived from (12) where we require that $f\langle x_2\rangle$ vanish at the boundary of $S2$ and use approximation (14):

$$\frac{dN_2}{dt}=\int_{S2}\frac{\partial f\langle x_2\rangle}{\partial t}dx_2,$$

$$=-\int_{S2}\frac{\partial}{\partial x_2}\left[f\langle x_2\rangle\frac{dx_2}{dt}\right]dx_2,$$

$$=0. \tag{15}$$

[2] Symbols are defined in the Appendix.

$$\frac{dL_2}{dt}=\int_{S2} x_2\frac{\partial f\langle x_2\rangle}{\partial t}dx_2,$$

$$=-\int_{S2} x_2\frac{\partial}{\partial x_2}\left[f\langle x_2\rangle\frac{dx_2}{dt}\right]dx_2,$$

$$=\int_{S2} f\langle x_2\rangle\frac{dx_2}{dt}dx_2, \tag{16}$$

$$=L_1\int_{S2} V(x_2|x_1)f\langle x_2\rangle dx_2. \tag{17}$$

$$\frac{dZ_2}{dt}=\int_{S2} x_2^2\frac{\partial f\langle x_2\rangle}{\partial t}dx_2,$$

$$=2\int_{S2} x_2 f\langle x_2\rangle\frac{dx_2}{dt}dx_2, \tag{18}$$

$$=2L_1\int_{S2} V(x_2|x_1)g\langle x_2\rangle dx_2. \tag{19}$$

We now choose the rate coefficient b_c for the accretion mode such that

$$\left.\frac{1}{x_2}\frac{dx_2}{dt}\right|_c=b_c(x_2,x_1)L_1, \tag{20}$$

where the subscript c denotes the continuous collection mode and the accretion process. By comparison with (14) it is evident that

$$b_c(x_2,x_1)=V(x_2|x_1)/x_2.$$

However, for reasons which will become apparent later we choose to define b_c such that

$$b_c(x_2,x_1)\equiv V(x_2|x_1)/(x_2+x_1), \tag{21}$$

where, for purposes of accretion the x_1 in the denominator is negligible, by definition. From (10) we have

$$b_c(r_2,r_1)=\frac{3}{4\rho}\left(\frac{r_2^2}{r_2^3+r_1^3}\right)\Delta v(r_2,r_1)Y_c^2(r_2,r_1). \tag{22}$$

Fig. 1 shows the values of $b_c(r_2,r_1)$ calculated by Reinhardt (1972) using the Y_c's mentioned above. The curves have a maximum near $r_2=120\,\mu$m, somewhat independently of r_1. A crude approximation to these curves is[3]

$$b_c(r_2,r_1)=10^4(-0.94+270r_1-0.24\ln r_2). \tag{23}$$

[3] As improved values of the collection kernel become available the values of the rate coefficient can be correspondingly revised or generalized.

Using (21) with $x_2\gg x_1$, we write (17) and (19) as

$$\left.\frac{1}{L_2}\frac{dL_2}{dt}\right|_c=\frac{L_1}{L_2}\int_{S2} b_c(x_2,x_1)x_2 f\langle x_2\rangle dx_2, \tag{24}$$

$$\left.\frac{1}{Z_2}\frac{dZ_2}{dt}\right|_c=\frac{2L_1}{Z_2}\int_{S2} b_c(x_2,x_1)x_2 g\langle x_2\rangle dx_2. \tag{25}$$

One measure of spectrum width is, from (8), the relationship of x_{f2} and x_{g2}. To calculate the changes in x_{f2} and x_{g2} we have from (4) and (5)

$$\left.\frac{1}{x_{f2}}\frac{dx_{f2}}{dt}\right|_c=\frac{1}{L_2}\frac{dL_2}{dt}, \tag{26}$$

$$\left.\frac{1}{x_{g2}}\frac{dx_{g2}}{dt}\right|_c=\frac{1}{Z_2}\frac{dZ_2}{dt}-\frac{1}{L_2}\frac{dL_2}{dt}. \tag{27}$$

Then, using (24) and (25) we have

$$\left.\frac{1}{x_{f2}}\frac{dx_{f2}}{dt}\right|_c=\frac{L_1}{L_2}\int_{S2} b_c(x_2,x_1)x_2 f\langle x_2\rangle dx_2, \tag{28}$$

$$\left.\frac{1}{x_{g2}}\frac{dx_{g2}}{dt}\right|_c=\frac{L_1}{L_2}\int_{S2} b_c(x_2,x_1)\left(\frac{2x_2}{x_{g2}}-1\right)x_2 f\langle x_2\rangle dx_2. \tag{29}$$

Now we define two specialized rate coefficients b_{cf}^* and b_{cg}^* in order that (28) and (29) may be put in the format of (20). Thus,

$$\left.\frac{1}{x_{f2}}\frac{dx_{f2}}{dt}\right|_c=b_{cf}^*(x_{g2},x_1)L_1, \tag{30}$$

$$\left.\frac{1}{x_{g2}}\frac{dx_{g2}}{dt}\right|_c=b_{cg}^*(x_{g2},x_1)L_1, \tag{31}$$

where we have used x_{g2} in place of x_2 in b_c^* since x_{g2} is the dominant value of x_2 in the integrands of (28) and (29). Then

$$b_{cf}^*(x_{g2},x_1)=\frac{1}{L_2}\int_{S2} b_c(x_2,x_1)x_2 f\langle x_2\rangle dx_2, \tag{32}$$

$$b_{cg}^*(x_{g2},x_1)=\frac{1}{L_2}\int_{S2} b_c(x_2,x_1)\left(\frac{2x_2}{x_{g2}}-1\right)x_2 f\langle x_2\rangle dx_2. \tag{33}$$

The values of b_{cf}^* and b_{cg}^* can be calculated for any particular b_c and $f\langle x_2\rangle$. (It may be possible that b_{cf}^* and b_{cg}^* can be parameterized in terms of x_1 and x_{g2} but such a pursuit is outside the scope of this discussion.)

In the special case, which according to Fig. 1 will hold roughly for $50\,\mu\text{m}\leqslant r_2\leqslant 200\,\mu$m and $r_{f1}\geqslant 8\,\mu$m, that b_c may be approximated by a constant value, we have from (32) and (33):

$$b_{cf}^*(x_{g2},x_1)\approx b_c(x_{g2},x_1), \tag{34}$$

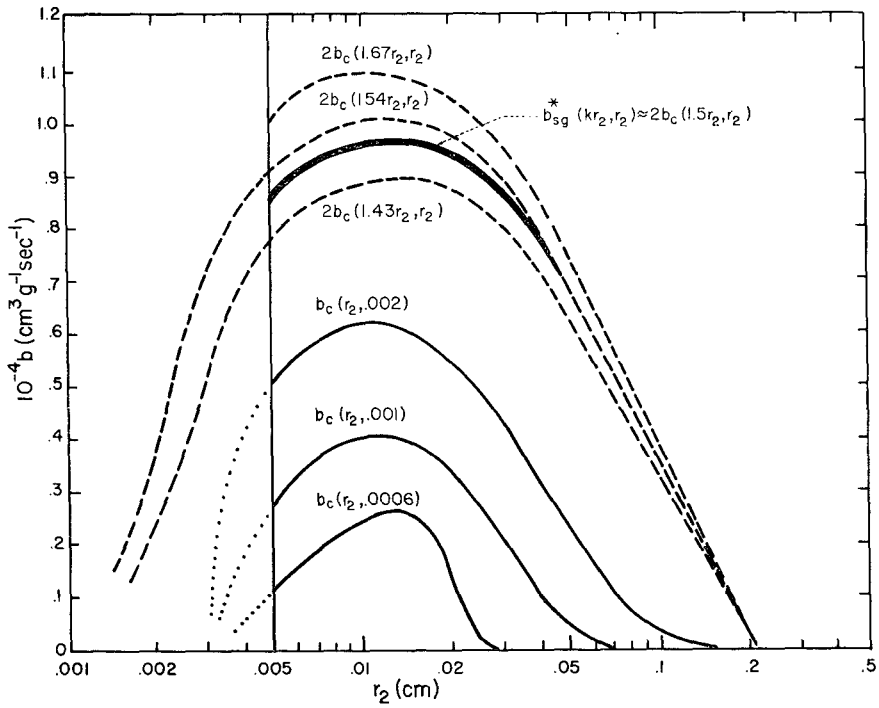

FIG. 1. The lower three curves give the values of $b_c(r_2,r_1)$ for the accretion parameterization calculated from Eq. (22) (from Reinhardt, 1972); the heavy line gives the values of $b^*_{sg}(r_{g2})$ for the self-collection parameterization (from Table 1); and the dashed lines are calculations of $2b_c(Kr_2,r_2)$ from Eq. (22) in an attempt to fit the heavy solid line.

$$b^*_{cg}(x_{g2},x_1)\approx b_c(x_{g2},x_1), \tag{35}$$

since x_{g2} is the dominant value of x_2 in the integrands of (32) and (33). In this case, b^*_{cf} and b^*_{cg} are identical and so are the logarithmic rates of change of x_{f2} and x_{g2} from (30) and (31). Since b_c is from (23) a relatively slowly varying function of x_2, the approximation (34) may not be too bad for some instances. However, only slight variations in the values in the integrand of (33) can cause it, and thus (35), to go to zero or even negative. Therefore, depending upon the particular circumstances, x_{g2} may increase, remain the same, or, in principal at least, even decrease during accretion.

One revealing clue to the behavior of $S2$ during accretion lies in the change in its relative variance. From (8) we have

$$\frac{d}{dt}(\text{var}\,x)=\frac{x_g}{x_f}\left(\frac{1}{x_g}\frac{dx_g}{dt}-\frac{1}{x_f}\frac{dx_f}{dt}\right), \tag{36}$$

which equals zero for the conditions of (34) and (35). Thus, there is little or no spreading in the accretion mode, which is what we might expect since it is based upon the continuous collection approximation. In a more exact way, the slight increase in b_c from $r_2=50\ \mu$m to $100\ \mu$m will be responsible for a slight spreading of $S2$ in this range since the larger drops will preferentially grow faster than the smaller drops. The opposite is true for $r_2>100\ \mu$m, and especially for $r_2>300\ \mu$m. Therefore, as the spectrum grows to include larger sized drops the effect of accretion will be to cause the spectrum to narrow. This lack of spreading, or even a decrease, resulting from accretion was seen in Part I.[4]

The change in relative variance may be written more completely by using (28) and (29) in (36), yielding

$$\frac{d}{dt}(\text{var}\,x)\Big|_c=\frac{x_g}{x_f}\frac{2}{L_2}\int_{S2}b_c(x_2,x_1)\left(\frac{x_2}{x_g}-1\right)x_2 f\langle x_2\rangle dx_2. \tag{37}$$

When b_c is a constant Eq. (37) is, from (2), (3) and (5), clearly zero, and in the region where b_c decreases with x_2 Eq. (37) is clearly negative, and vice-versa.

In summary, accretion may be described in terms of the parameterized Eqs. (30), (31), (32) and (33). Being a generalization of the continuous collection approximation, accretion does not contain the inherent spreading mechanism of stochastic collection. Although x_f and x_g will be affected by positive or negative values of the slope of the rate coefficient, i.e., the value of the derivative $\partial b_c/\partial x_2$, the result at best can slowly broaden the

[4] Although (8) and (36) properly relate to a linear x axis, we feel it is best to retain this definition of variance since it incorporates physically meaningful values like L and Z, and with judgement we apply its qualitative results to the ln radius plots. We note that $1+\text{var}\,x=x_g/x_f$, and $\ln(1+\text{var}\,x)=\ln x_g-\ln x_f$. Thus the difference $(\ln x_g-\ln x_f)$ on the ln plots is proportional to the ratio x_g/x_f which is a measure of the relative variance.

spectrum to var $x = 1$. This will be discussed in more detail in Part IV.

4. Large-hydrometeor self-collection

Two features contained in the growth patterns shown in Part II appear with astonishing regularity. These are the shape of $S2$ and the growth rate of r_g after $r_g > 50$ μm. This is the range where $r_g \approx r_{g2}$. Once $S2$ begins to take form it soon dominates the growth patterns and retains little memory for the initial characteristics of $S1$. As $S1$ diminishes, this growth pattern is quite independent of the accretion mode. It is a pattern of growth similar to Golovin's (1963) asymptotic solution of the stochastic collection equation, as discussed by Berry (1967). It is a mode that is due to the self-collection of $S2$ hydrometeors. This mode is responsible for both the regular spread of $S2$ and the rapid growth of r_{g2}. Because it seeks an asymptotic form and is dependent only upon itself, the hydrometeor self-collection mode is relatively easy to parameterize.

As indicated by Berry (1967) this growth mode may be represented by a form similar to (20), i.e., by

$$\left.\frac{1}{x_{g2}}\frac{dx_{g2}}{dt}\right|_s = b^*_{sg}(x_{g2})L_2, \tag{38}$$

where b^*_{sg} is the stochastic rate coefficient for x_{g2}, and the subscript s denotes the stochastic collection mode and the self-collection process. This equation differs from (20) in that it depends on L_2 rather than L_1 and b^*_{sg} is a function only of x_{g2}. In the case of Golovin's solution, b^*_{sg} was a constant. Here, we will evaluate b^*_{sg} on the basis of the calculations performed.[5]

The growth rate of x_{g2} in the calculations described here is the sum of the contributions of the accretion (31) and self-collection (38) processes. Thus,

$$\left.\frac{1}{x_{g2}}\frac{dx_{g2}}{dt}\right|_{c+s} = b^*_{cg}(x_{g2},x_1)L_1 + b^*_{sg}(x_{g2})L_2. \tag{39}$$

Reinhardt (1972) defined a total $b_g(x_g)$ based upon the total x_g and the total water content L. Using an equation similar to (20) and (38), namely

$$\left.\frac{1}{x_g}\frac{dx_g}{dt}\right|_{c+s} = b_g(x_g)L, \tag{40}$$

he used the figures shown in Part II to calculate values of $b(x_g)$, here reproduced in Fig. 2. We have only to properly relate the values of (39) and (40) to calculate $b^*_{sg}(x_{g2})$.

[5] In retrospect, a more accurate and straightforward way would be to eliminate $S1$ and re-run the calculations with several initial $S2$'s with $L_2 = 10^{-6}$, but it was not clear at the outset of these calculations just what parameterization pattern would result.

First we write x_g in terms of x_{g1} and x_{g2}. Since both L and Z are extensive variables we have

$$x_g L = x_{g1}L_1 + x_{g2}L_2, \tag{41}$$

$$L = L_1 + L_2. \tag{42}$$

Since x_{g1} and L are constant and $x_{g2} \gg x_{g1}$, we have

$$\left.\frac{1}{x_g}\frac{dx_g}{dt}\right|_{c+s} = \frac{1}{x_g L}\left[(x_{g2}-x_{g1})\left.\frac{dL_2}{dt}\right|_c + L_2\left.\frac{dx_{g2}}{dt}\right|_{c+s}\right]$$

$$= \frac{x_{g2}}{x_g}\frac{1}{L}\left.\frac{dL_2}{dt}\right|_c + \frac{L_2}{L}\frac{1}{x_g}\left.\frac{dx_{g2}}{dt}\right|_{c+s}.$$

Using (26) and (30), (39) and (40), we now have

$$b_g(x_g)L$$

$$= \frac{x_{g2}}{x_g}\frac{L_2}{L}b^*_{cf}(x_{g2},x_1)L_1 + \frac{x_{g2}}{x_g}\frac{L_2}{L}[b^*_{cg}(x_{g2},x_1)L_1 + b^*_{sg}(x_{g2})L_2]$$

$$= \frac{x_{g2}}{x_g}\frac{L_2}{L}[b^*_{cf}(x_{g2},x_1)L_1 + b^*_{cg}(x_{g2},x_1)L_1 + b^*_{sg}(x_{g2})L_2].$$

Since we will use $x_{g1}L_1 \ll x_{g2}L_2$, the coefficient on the right-hand side may be equated to unity, and we have, finally

$$b_g(x_g)L = [b^*_{cf}(x_{g2},x_1) + b^*_{cg}(x_{g2},x_1)]L_1 + b^*_{sg}(x_{g2})L_2. \tag{43}$$

To evaluate $b_{sg}(x_{g2})$ from (43) we select the case of Fig. 6, Part II, where $r_{f0} = 18$ μm and var $x = 1$, in order that L_1 and the errors introduced in the evaluation of b^*_{cf} and b^*_{cg} will be small. Using the approximations (34) and (35), Eq. (43) becomes

$$b_g(x_g) = 2b_c(x_{g2},x_1)(L_1/L) + b^*_{sg}(x_{g2})(L_2/L). \tag{44}$$

We now use curve (18,0) of Fig. 2 to evaluate $b_g(r_g)$, Fig. 1 to evaluate $b_c(r_{g2},r_1)$, Fig. 6 of Part II to evaluate (L_2/L) and thus (L_1/L), and calculate $b^*_{sg}(r_{g2})$ from (44). Data relevant to the calculation is given in Table 1.

Values of $b^*_{sg}(r_{g2})$ from Table 1 are plotted in Fig. 1. For comparison we have also plotted values of $2b_c(Kr_2,r_2)$ according to (22) for several values of K. If the values of $b^*_{sg}(r_{g2})$ are an indication of the predominant collection occurring in $S2$, we may conclude that the $(1.5r_2,r_2)$ is the dominant mode for stochastic collection within $S2$. [This also corresponds to the conclusions drawn from Fig. 11 of Berry (1967)]. The close fit of the data of Table 1 to the $(1.5r_2,r_2)$ curve of Fig. 1 seems remarkable.

It is interesting that it takes twice the value of b_c to approximate b^*_s. The reason for this will be shown below. But first it is necessary to derive a formula for the evaluation of b^*_s. We do this as follows. Since from (5) with L_2 constant,

$$\left.\frac{1}{x_{g2}}\frac{dx_{g2}}{dt}\right|_s = \left.\frac{1}{Z_2}\frac{dZ_2}{dt}\right|_s, \tag{45}$$

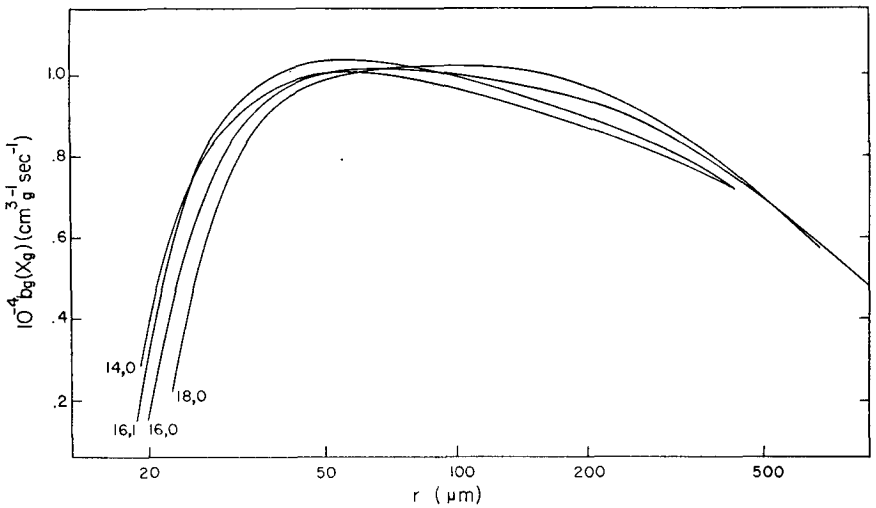

FIG. 2. The factor $b_g(x_g)$ of the instantaneous rate of change of x_g as a function of $r_g(x_g)$ for initial conditions given by (r_g,ν) where var $x=(1+\nu)^{-1}$.

we use (3) to get

$$\frac{1}{Z_2}\frac{dZ_2}{dt}\bigg|_s=\frac{1}{Z_2}\int_{x_0}^{\infty}x^2\frac{\partial f}{dt}dx,$$

and substitute Eq. (9):

$$\frac{1}{Z_2}\frac{dZ_2}{dt}\bigg|_s=\frac{1}{Z_2}\int_{x_0}^{\infty}x^2dx\int_{x_0}^{x/2}f\langle x-x'\rangle V(x-x'|x')f\langle x'\rangle dx$$

$$-\frac{1}{Z_2}\int_{x_0}^{\infty}x^2dx\int_{x_0}^{\infty}f\langle x\rangle V(x|x')f\langle x'\rangle dx'. \quad (46)$$

We treat the first integral I_1, of (46) as follows:

$$Z_2I_1=\frac{1}{2}\int_{x_0}^{\infty}dx\int_{x_0}^{x}dx'\,x^2f\langle x-x'\rangle V(x-x'|x')f\langle x'\rangle,$$

$$=\frac{1}{2}\int_{x_0}^{\infty}dx'\int_{x_0}^{\infty}dx\,x^2f\langle x-x'\rangle V(x-x'|x')f\langle x'\rangle.$$

Substituting $x+x'$ for x and using the symmetry of $V(x|x')$, we have

$$Z_2I_1=\frac{1}{2}\int_{x_0}^{\infty}dx'\int_{x_0}^{\infty}dx\,(x+x')^2f\langle x\rangle V(x|x')f\langle x'\rangle,$$

$$=\int_{x_0}^{\infty}dx\int_{x_0}^{\infty}dx'\,x^2f\langle x\rangle V(x|x')f\langle x'\rangle$$

$$+\int_{x_0}^{\infty}dx\int_{x_0}^{\infty}dx'\,xx'f\langle x\rangle V(x|x')f\langle x'\rangle.$$

With reinsertion in (46) we have

$$\frac{1}{x_{g2}}\frac{dx_{g2}}{dt}\bigg|_s=\frac{1}{Z_2}\int_{x_0}^{\infty}dx\int_{x_0}^{\infty}dx'xx'f\langle x\rangle V(x|x')f\langle x'\rangle. \quad (47)$$

Dropping the integral limits and substituting (21)[6] we use (38) to write for $b^*_{sg}(x_{g2})$:

$$b^*_{sg}(x_{g2})=\frac{2}{Z_2L_2}\int_{S2}x^2f\langle x\rangle dx\int_{S2}b_c(x,x')x'f\langle x'\rangle dx', \quad (48)$$

where the coefficient 2 arises because of the $(x+x')$ term in (21) and the resulting symmetry of the integrand.

The correct b^*_{sg} is now given by Eq. (48). The values in Table 1 result from derivations from the numerical experiments. Values of b^*_{sg} derived (but not shown here) from the other numerical experiments are similar. This may be attributed to the facts (i) that all the calculations use the same b_c, and (ii) that the $S2$ spectral shape in all cases approaches the same form, independent of $S1$ and dependent only on b_c in the $S2$ range. Thus (48), which is normalized by Z_2 and L_2 and thus dependent only on b_c and the shape and position of $f\langle x\rangle$, will produce similar b^*_{sg} for all cases.

We can now apply (47) to the simple kernels, discussed by Berry (1967) and Scott (1968), which produce analytic solutions to the stochastic collection equation. If $b_c=b_2$, a constant, we have the Golovin (1963) kernel which is so useful because it is similar to realistic kernels for intermediate sized drops, say 40 μm $\leqslant r\leqslant$ 400 μm. Then

$$V(x|x')=b_2(x+x'), \quad (49a)$$

[6] This was the reason for keeping the symmetry in the definition (21).

TABLE 1. Evaluation of b^*_{sg} by (44) using b_g values from Fig. 2 for the curve (18,0).

r_g ($\times 10^4$)	r_{g2} ($\times 10^4$)	(L_2/L)	(L_1/L)	b_g ($\times 10^{-4}$)	b_c ($\times 10^{-4}$)	$\left(2\frac{L_1}{L}b_c\right)$ ($\times 10^{-4}$)	$\left(b-2\frac{L_1}{L}b_c\right)$ ($\times 10^{-4}$)	b^*_{sg} ($\times 10^{-4}$)
50	62	0.50	0.50	0.98	0.53	0.53	0.45	0.90
60	71	0.57	0.43	1.00	0.57	0.49	0.51	0.90
100	110	0.75	0.25	1.02	0.61	0.30	0.72	0.96
150	158	0.85	0.15	1.00	0.59	0.18	0.82	0.96
200	200	0.90	0.10	0.98	0.54	0.11	0.87	0.96
300	300	0.95	0.05	0.86	0.41	0.04	0.82	0.86
500	500	0.98	0.02	0.72	0.22	0.01	0.71	0.73

$$\frac{1}{x_{g2}}\frac{dx_{g2}}{dt}\bigg|_{s,2} = 2b_2L_2. \tag{49b}$$

Comparing (49b) with (38) we see that

$$b^*_{sg} = 2b_2. \tag{49c}$$

Thus we have a clear analytic reason for b^*_{sg} being approximately twice the value of b_c in the intermediate sized regions of Fig. 1.

Physically, the factor of 2 in (49b) is brought about by the fact that in the stochastic process two drops are eliminated for every one created (as opposed to the continuous approximation where the identity of the larger drop is preserved) and this results in an overall movement of x_{g2} at twice the rate of the continuous process.

It is instructive to look at the two other kernels giving analytic solutions. The first is somewhat characteristic of growth in the early life of a spectrum when the tail stretches out to larger radii and before the "second maximum" (Berry, 1967) forms:

$$V(x|x') = b_1xx', \tag{50a}$$

$$\frac{1}{x_{g2}}\frac{dx_{g2}}{dt}\bigg|_{s,2} = x_{g2}b_1L_2. \tag{50b}$$

Here there is no coefficient 2, but the growth rate is one which is proportional to x_{g2}. This will result in a long shallow tail which extends to larger drops at an ever-increasing rate. This is a situation which would rapidly distribute all the water mass on a single large drop and therefore the use of a continuous density function soon becomes unphysical. In the case of cloud drops, however, the kernel at intermediate sized drops becomes more similar to that of (49) and this interrupts the tail-extending growth of (50) and results in the formation of the "second hump."

The final analytic kernel is somewhat representative of the growth of the spectrum at radii well above 400 μm. In this region the kernel no longer increases dramatically with drop size but becomes constant and then gradually decreases in value. This growth region may be represented by[7]

$$V(x|x') = b_3, \tag{51a}$$

$$\frac{1}{x_{g2}}\frac{dx_{g2}}{dt}\bigg|_{s,3} = \frac{1}{x_{g2}}b_3L_2. \tag{51b}$$

Here the growth rate slows with increasing x_{g2}, and the spectrum becomes narrower and taller. All of the above growth patterns were shown in Part II.

Using arguments similar to those above produces not only the well-known result that $(dL_2/dt)_s = 0$, but also the formula for the rate of change of N_2 and thus x_{f2}:

$$\frac{1}{x_{f2}}\frac{dx_{f2}}{dt}\bigg|_{s} = \frac{1}{2N_2}\int_{S2}dx\int_{S2}dx'\,f\langle x\rangle V(x|x')f\langle x'\rangle, \tag{52}$$

from which, defining $b^*_{sf}(x_{g2},x_{f2})$, we have, using (21),

$$\frac{1}{x_{f2}}\frac{dx_{f2}}{dt}\bigg|_{s} = b^*_{sf}(x_{g2},x_{f2})L_2, \tag{53}$$

$$b^*_{sf}(x_{g2},x_{f2}) = \frac{1}{N_2L_2}\int_{S2}xf\langle x\rangle dx\int_{S2}b_c(x,x')f\langle x'\rangle dx'. \tag{54}$$

We notice that (52) and (54) lacks an xx' compared to (47) and (48), respectively, and therefore weights the value of $b_c(x,x')$ toward smaller radii (where, incidentally, x_f resides). We have used this as the reasons for making b^*_{sf} a function of x_{f2}, and b^*_{sg} a function of x_{g2}.

Evaluating (52) for the same three analytic kernels as we did for (47), we find for $V(x|x') = b_1xx'$, $b_2(x+x')$, b_3, respectively:

$$\frac{1}{x_{f2}}\frac{dx_{f2}}{dt}\bigg|_{s,1} = \tfrac{1}{2}x_{f2}b_1L_2, \tag{55}$$

$$\frac{1}{x_{f2}}\frac{dx_{f2}}{dt}\bigg|_{s,2} = b_2L_2, \tag{56}$$

$$\frac{1}{x_{f2}}\frac{dx_{f2}}{dt}\bigg|_{s,3} = \frac{1}{2}\frac{1}{x_{f2}}b_3L_2. \tag{57}$$

[7] Notice that b_1, b_2 and b_3 have different units.

Thus, the growth rates for x_{f2} are one-half those of x_{g2} (for equal x_{f2} and x_{g2}). The subscripts designate regions 1, 2, 3 corresponding to the analytic kernels with b_1, b_2, b_3, respectively.

Because of the gradual slowing of the growth rates of both x_{f2} and x_{g2} as they progress from the regions of b_1 to b_2, and b_2 to b_3, we can conclude

$$[x_a b_1 = 2b_2 = b_3/x_c]_s, \tag{58}$$

where x_a, x_c can be either x_{f2} or x_{g2}, and x_a and x_c are the lower and upper bounds of the region valid for b_2. Thus, the growth rate increases as x_{f2}, x_{g2} grows to x_a, then holds constant until x_{f2}, x_{g2} reaches x_c, and decreases thereafter.

In summary, the logarithmic growth rate of x_{g2} due to self-collection of $S2$ is proportional to a rate coefficient and the total mass of particles in $S2$. This rate coefficient has been given an analytic formula and has been evaluated on the basis of the results of the numerical experiments. This stochastic mode rate coefficient has been found to be approximately twice that of the continuous mode rate coefficient for intermediate sized drops and many times larger for the large sized drops. A similar, but different rate coefficient has been developed for the mean mass x_{f2}.

The growth pattern of drops with a realistic collection kernel has been compared to a sequence of three analytic kernels, the first causing rapid spreading, the second generating the Golovin asymptotic form, and the third causing the spectrum to slow down its growth and narrow. The analytic kernel representing the intermediate situation has been the model for our definition of the basic rate coefficient. This sequence of kernels has been used as an explanation of the formation of the "second maximum."

5. Conclusions

The accretion process, by which large hydrometeors capture the smaller cloud droplets, has been given an exact parametric formulation. The formulation shows, in correspondence with the data of Parts I and II, that accretion has a narrowing effect on the large hydrometeor distribution and therefore cannot be responsible for the Marshall–Palmer distribution of raindrops. The primary function of accretion is to transfer water mass from the cloud droplet population to the large hydrometeor population.

The large-hydrometeor self-collection process, by which the large hydrometeors combine to form larger hydrometeors, has also been given a parametric formulation. By using the data of Parts I and II the stochastic mode rate coefficient for self-collection has been evaluated and found to be approximately twice the continuous mode rate coefficient for accretion for intermediate sized drops and many times larger for the larger drops. This mode is shown to be responsible for all essential spreading of the large-hydrometeor spectrum, and in balance with hydrometeor breakup is expected to produce the Marshall–Palmer distribution. The rate at which self-collection proceeds is proportional to the large-hydrometeor water content, which in turn is controlled by accretion.

The rate coefficients for each process have been related to the collection kernel, eliminating the requirement to generate new data via a full numerical solution to the stochastic collection equation for each slight change in the collection kernel. The rate coefficient for stochastic collection has been found to be related to the kernel for the capture of predominate sized drops by drops 1.5 times their diameter.

This method of parameterization includes the essential interactive features of cloud particle growth and can readily be extended to the ice and ice-water phases.

The formation of the "second maximum" found by Berry (1967) has been explained.

Acknowledgments.[8] The principal author wishes to thank the following for their part in this research: Dr. W. A. Mordy for the original initiation and continued encouragement of this research Dr. Pierre; St.-Amand for the stimulus provided by his many invitations to lecture at the Naval Weapons Center and to participate in the NWC field experiments; Dr. Larry G. Davis and Dr. Archie Kahan for the opportunity to participate in various conferences and field programs; and Dr. Dan Gillespie for comments on the manuscript.

The research is an extension of the research reported in Parts I and II, which was supported by the Atmospheric Sciences Section, National Science Foundation, under Grant GA-21350.

APPENDIX

List of Symbols

b	total rate coefficient, accretion plus self-collection
b_c	rate coefficient for accretion only
b_s	rate coefficient for self-collection only
f	number density function
g	mass density function
L	liquid water content
N	total number density
r	droplet radius
r_f	radius corresponding to $x_f = L/N$
r_g	radius corresponding to $x_g = Z/L$
$S1$	the small hydrometeor or "cloud water" portion of the spectrum
$S2$	the large hydrometeor portion of the spectrum
V	collection kernel
var r	relative variance of the spectrum with respect to radius

[8] For Parts III and IV.

$\text{var}\, x$	relative variance with respect to mass
x	droplet mass
x_f	mean mass of the number density function
x_g	mean mass of the mass density function
Y_c	linear collision efficiency
Z	spectral radar reflectivity, the second mass moment of the number density function
Δv	difference in terminal fallspeeds
ρ	density of pure water

REFERENCE

Berry, E. X, 1967: Cloud droplet growth by collection. *J. Atmos. Sci.*, **24**, 688–701.

——, and R. L. Reinhardt, 1974a: An analysis of cloud drop growth by collection: Part I. Double distributions. *J. Atmos. Sci.*, **31**, 1814–1824.

——, and ——, 1974b: An analysis of cloud drop growth by collection: Part II. Single initial distributions. *J. Atmos. Sci.*, **31**, 1825–1831.

Golovin, A. M., 1963: The solution of the coagulating equation for cloud droplets in a rising air current. *Bull. Akad. Sci. USSR, Geophys. Ser.*, No. 5, 482–487.

Kessler, E., 1969: On the distribution and continuity of water substance in atmospheric circulations. *Meteor. Momogr.*, **10**, No. 32, 84 pp.

Reinhardt, R. L., 1972: An analysis of improved numerical solutions to the stochastic collection equation for cloud droplets. Ph.D. dissertation, University of Nevada.

Scott, W. T., 1968: Analytic studies of cloud droplet coalescence 1. *J. Atmos. Sci.*, **25**, 54–65.